Engineering Journal of Qatar University, Vol. 2, 1989.

"BEHAVIOUR OF GREY CAST IRON UNDER COMBINED BENDING AND TENSION"

By

Galal S. A. Shawki

Professor and Dean,
Faculty of Engineering, Qatar University,
Doha, Qatar, Arabian Gulf.

ABSTRACT

This paper deals with the strength of grey cast iron components subjected to combined bending and tension, this case of loading being met in C–frames and clamps, crane hooks and various eccentrically–loaded protruding machine parts.

Specimens of rectangular as well as trapezoidal sections, made of flake graphite cast iron, were tested under conditions of eccentric loading. With due consideration of non-linearities and inequalities in stress-strain relations in tension and compression, stress distribution for these sections was obtained from strain measurements.

The ratio of bending to tensile stress components is herein shown to play a significant role in locating the neutral plane and in identifying the dominating failure stress. The value 2, for this ratio, is shown to draw some demarkation border between the two modes of fracture encountered in the tests.

The apparent superiority of bending strength over tensile strength is herein attributed to the widely differing stress-strain relations in tension and compression.

1 – INTRODUCTION

In previous papers by the author [1,2], results of experiments conducted on lamellar graphite grey cast iron blocks, loaded in pure bending, were reported. Strain measurements indicated that longitudinal strains varied linearly along the height of the specimen until fracture, thus confirming the traditional speculation that plane sections remain plane under strain.

Due to the non-linearity of the stress-strain relationship, however, the neutral axis moves away from the centroidal axis towards the compression side, Fig. (1), which shift is enhanced with increased loading.

While on the compression side, the simple flexural formula:

$$\sigma_b = \frac{M.\ Y}{I} \qquad (1)$$

may well be applied with reasonable accuracy, this formula does not hold true for the extension side [1].

Should cast iron specimens be acted upon by a tensile load P superposed on the bending moment M, e.g. by application of a longitudinal eccentric load, the stress picture would assume the form shown in Fig. (2) in which two stress profiles may be noted, viz.:

1) Linear stress profile which emerges from the simple flexural formula: $\sigma_b = M.\ Y/I$, this being applicable in cases of identical material behaviour in tension and compression with linear stress-strain relationship.

2) Non-linear stress profile which evolves from the shift of neutral axis away from the centroidal axis towards the compression side, as a result of non-linearities and inequalities in stress-strain relations in tension and compression.

2 – EXPERIMENTAL SET-UP

The test rig used for present investigations comprises a 600 KN Universal testing machine with flat grips in which are inserted the ends of simple eccentric specimens of cranked form, Fig. (3). Two versions of the eccentric portion of the test specimen are herein dealt with, namely:

a) A straight rectangular cross section measuring 21 x 45 mm with eccentricity values measured from the axis of loading of 15 and 40 mm respectively,

b) A trapezoidal cross section measuring 25/45 x 45 mm with eccentricity values of 6, 8, 45 and 88 mm respectively, Fig. (3).

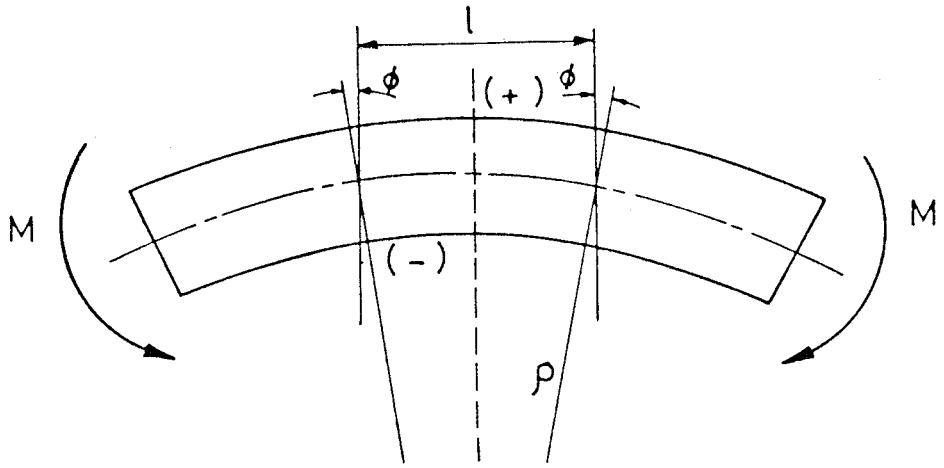

(a) – Strain Distribution

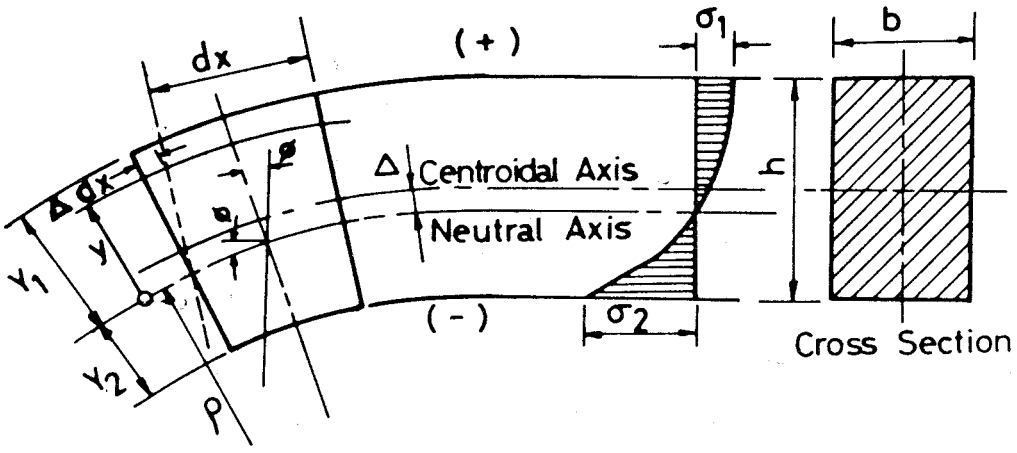

(b) – Stress Distribution

Fig. (1) – Strain and stress distributions under pure bending.

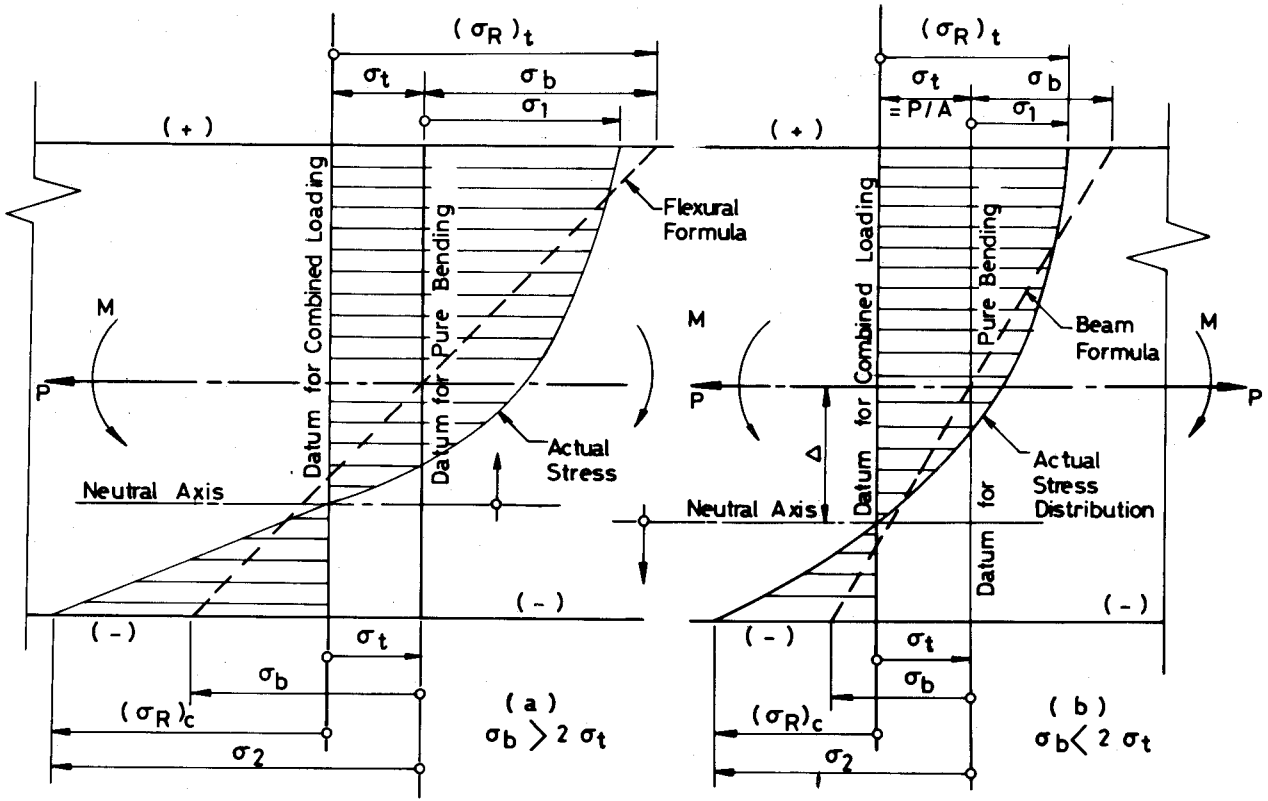

Fig. (2) – Stress distribution under combined bending and tensile load.

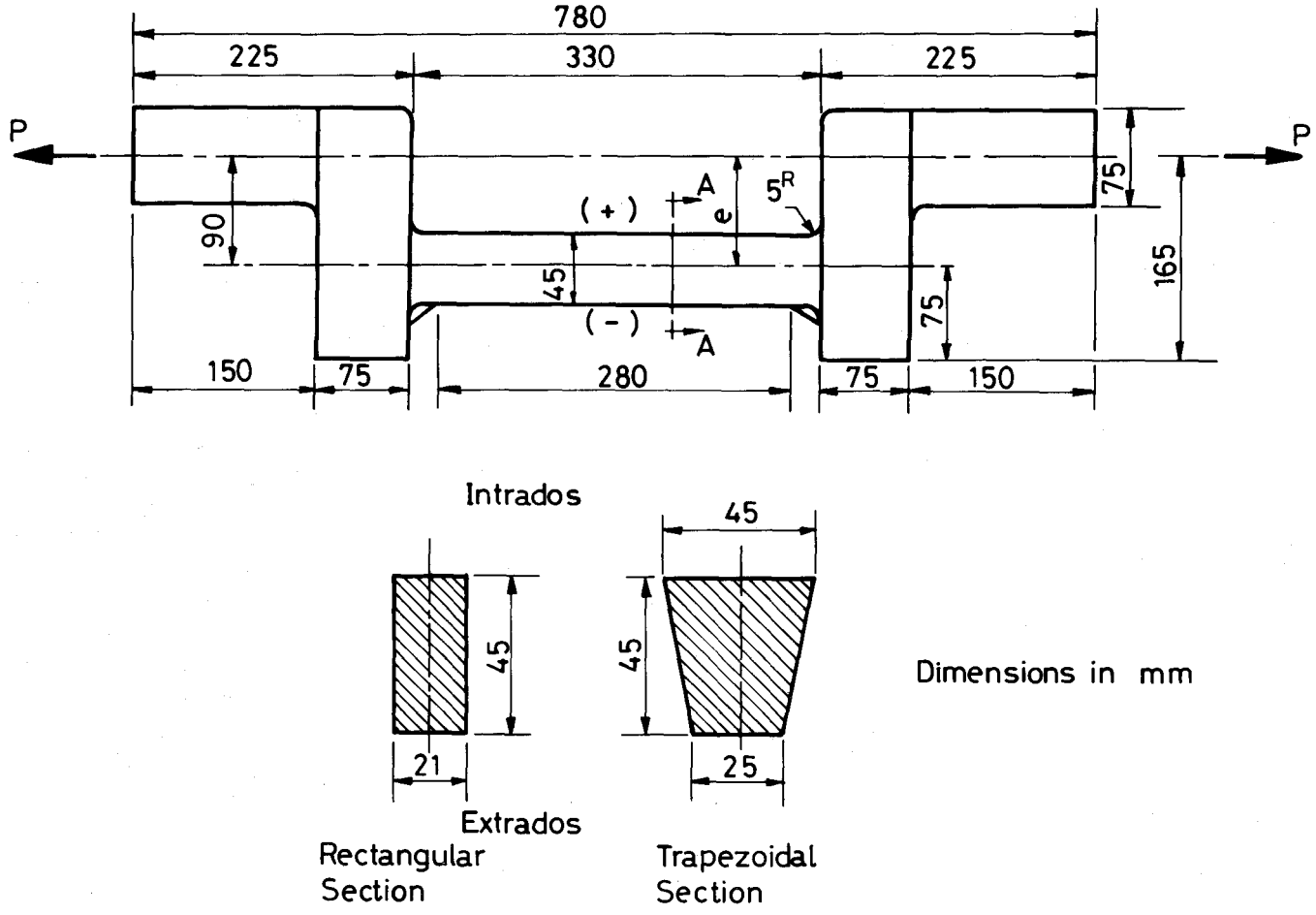

Fig. (3) - Dimensional details of test specimens.

Table (1) - Chemical Composition and Mechanical Properties of Tested Grey Cast Iron.

Specimen Designation	Chemical Composition					S_c*	Mechanical Properties			Remarks
	%C	%Mn	%S	%P	%Si		$(\sigma_u)_t$ MPa	$(\sigma_u)_c$ MPa	HB	
T_1 , C_1	3.0	0.75	0.065	0.2	1.06	0.78	200	640	212	Used in tension and compression specimens
T_2 , C_2	3.5	0.70	0.065	0.35	3.73	1.18	185	743	197	
T_3 , C_3	3.15	0.75	0.065	0.25	2.3	0.92	182	695	207	
B_1	3.5	0.70	0.06	0.076	2.06	0.98	120	480	149	Used in bending specimens
B_2	3.1	0.62	0.085	0.175	2.3	0.9	175	482	197	
F_1	3.0	0.42	0.085	0.09	3.97	1	122.5	459	149	Used in fracture specimens

* Degree of Saturation as defined by Felix (W. Felix: "The Modulus of Elasticity as an Aid to Assessing the Quality of Cast Iron", Sulzer Technical Review, 4, 1964).

Table (1) displays the chemical composition as well as the mechanical properties of grey cast iron specimens tested.

Elastic strain gauges (of type SR4) were located and distributed in a longitudinal order across the eccentric section, with two strain gauges fixed at the two limiting surfaces with a view to measuring the extremities of induced strains.

For each specimen, strains were measured and recorded at load increments of some 5 KN up to fracture.

3 - TEST RESULTS

3.1 - Stress Distribution

Stress patterns for both rectangular and trapezoidal specimens are displayed in Figures (4) to (9) for various values of load eccentricity [e]. For specimens with rectangular cross section, it can be readily seen that the resultant stress at the extension side $(\sigma_R)_t = (\sigma_t + \sigma_1)$ is the dominating stress which dictates fracture, Figs. (4) and (5).

Test results for specimens with trapezoidal cross section, Figs. (6) and (7), show that the stress, on the compression side, assumes positive and zero values for e = 6 and 8 mm respectively.

For the special case shown in Fig. (7), $|\sigma_2| \approx |\sigma_t|$ with the result that the neutral axis is so shifted as to almost coincide with the extreme compression fibre.

For higher load eccentricity (e = 45 and 88 mm), negative stress values appear, as expected, on the compression side, Figs. (8) and (9).

3.2 - Examination of Fractured Specimens

Plates (1) and (2) display typical fractured specimens of trapezoidal section after being subjected to combined tensile and bending loads.

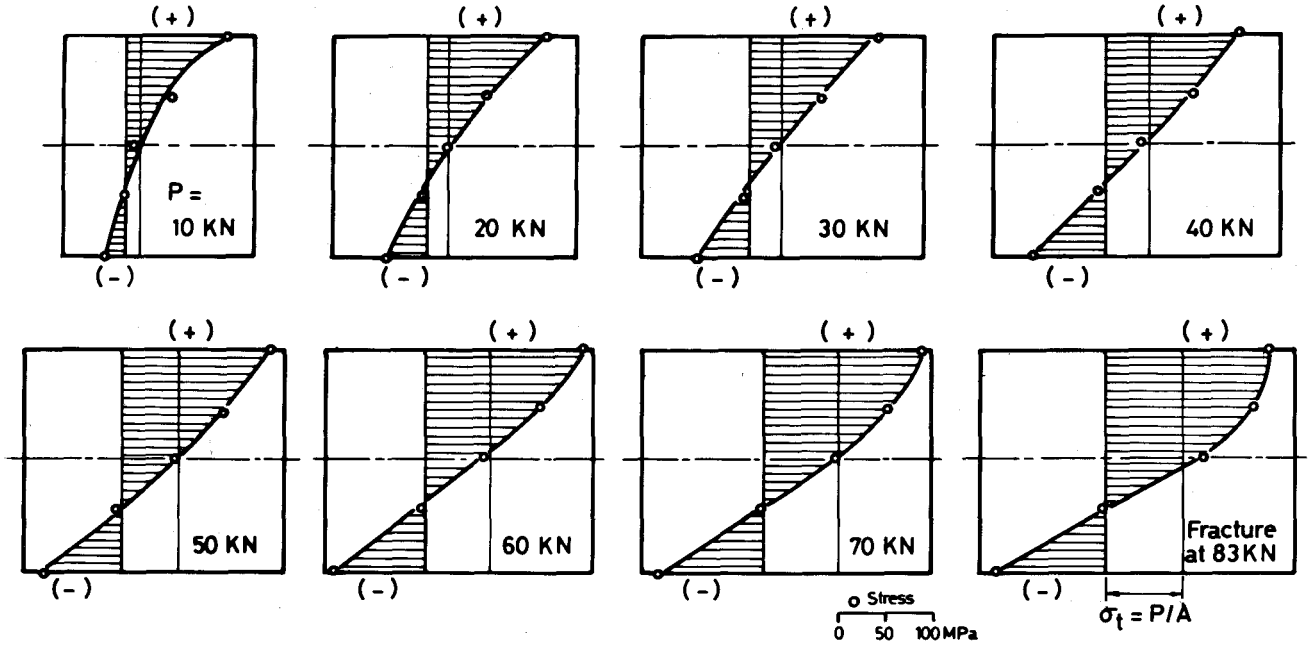

Fig. (4) – Stress distribution for rectangular specimens subjected to eccentric axial loading (Eccentricity e = 15 mm) (Case of $| \sigma_2 / \sigma_t | > 2$)

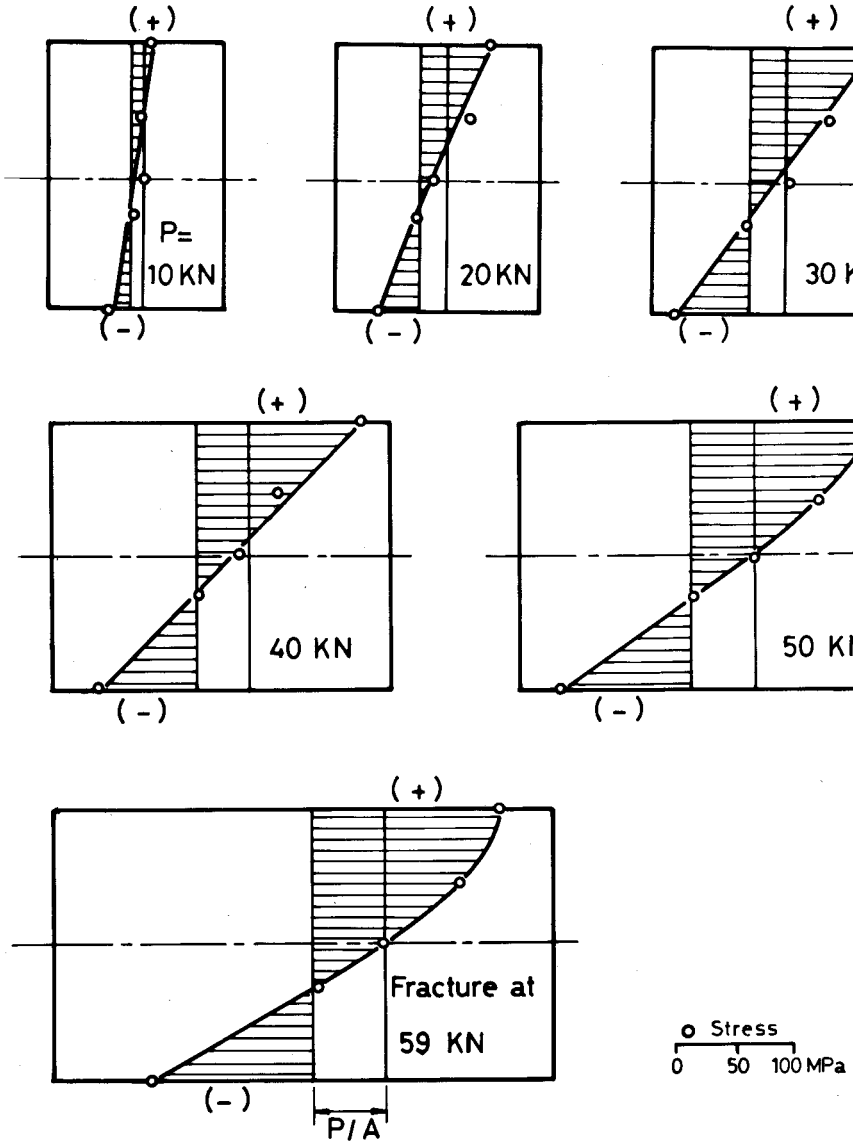

Fig. (5) – Stress distribution for rectangular specimens subjected to eccentric axial load (e = 40 mm)
(Case of $| \sigma_2 / \sigma_t | > 2$)

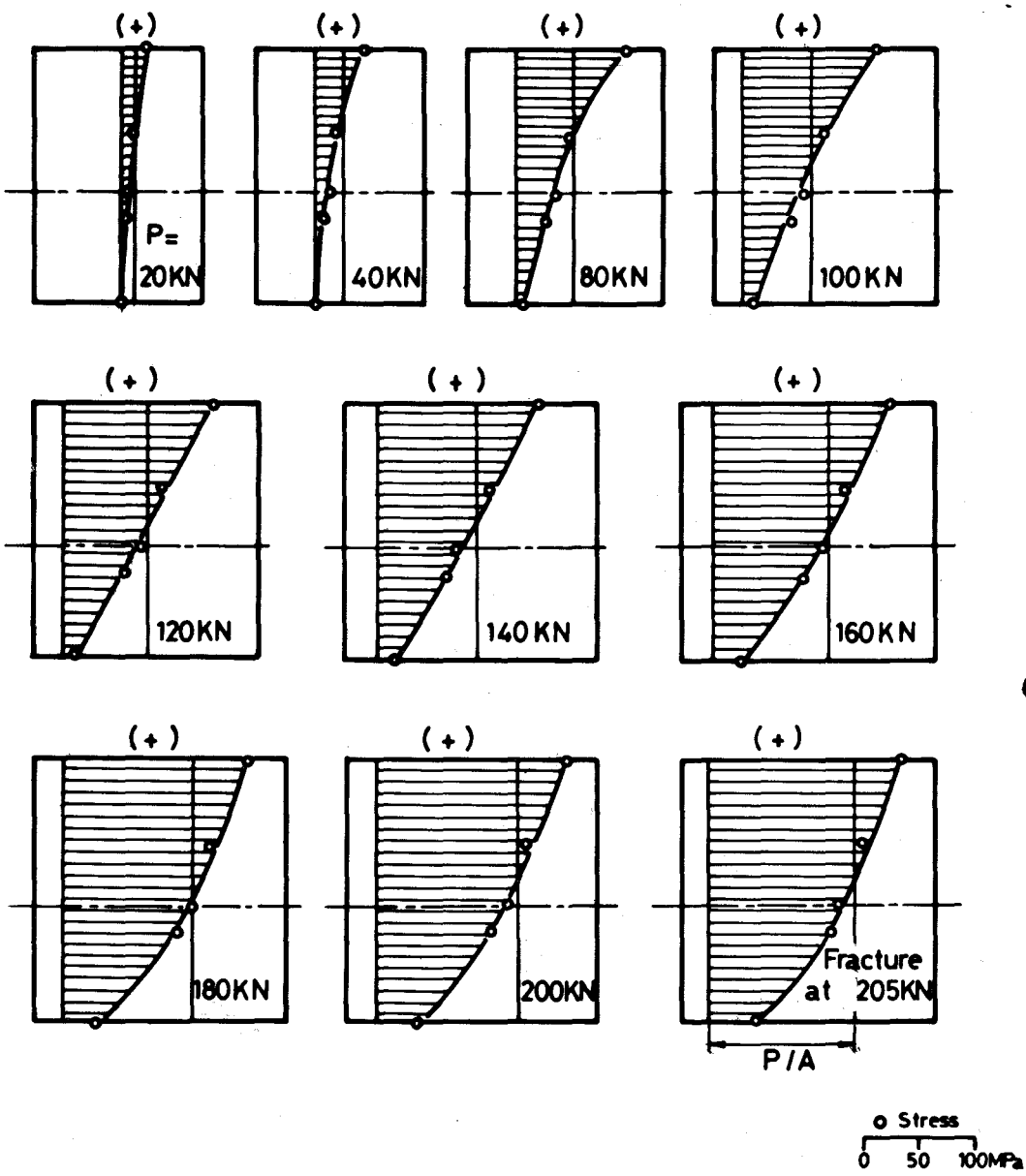

Fig. (6) – Stress distribution for trapezoidal specimens subjected to eccentric axial load (e = 6 mm)
(Case of $| \sigma_2 / \sigma_t | < 1$)

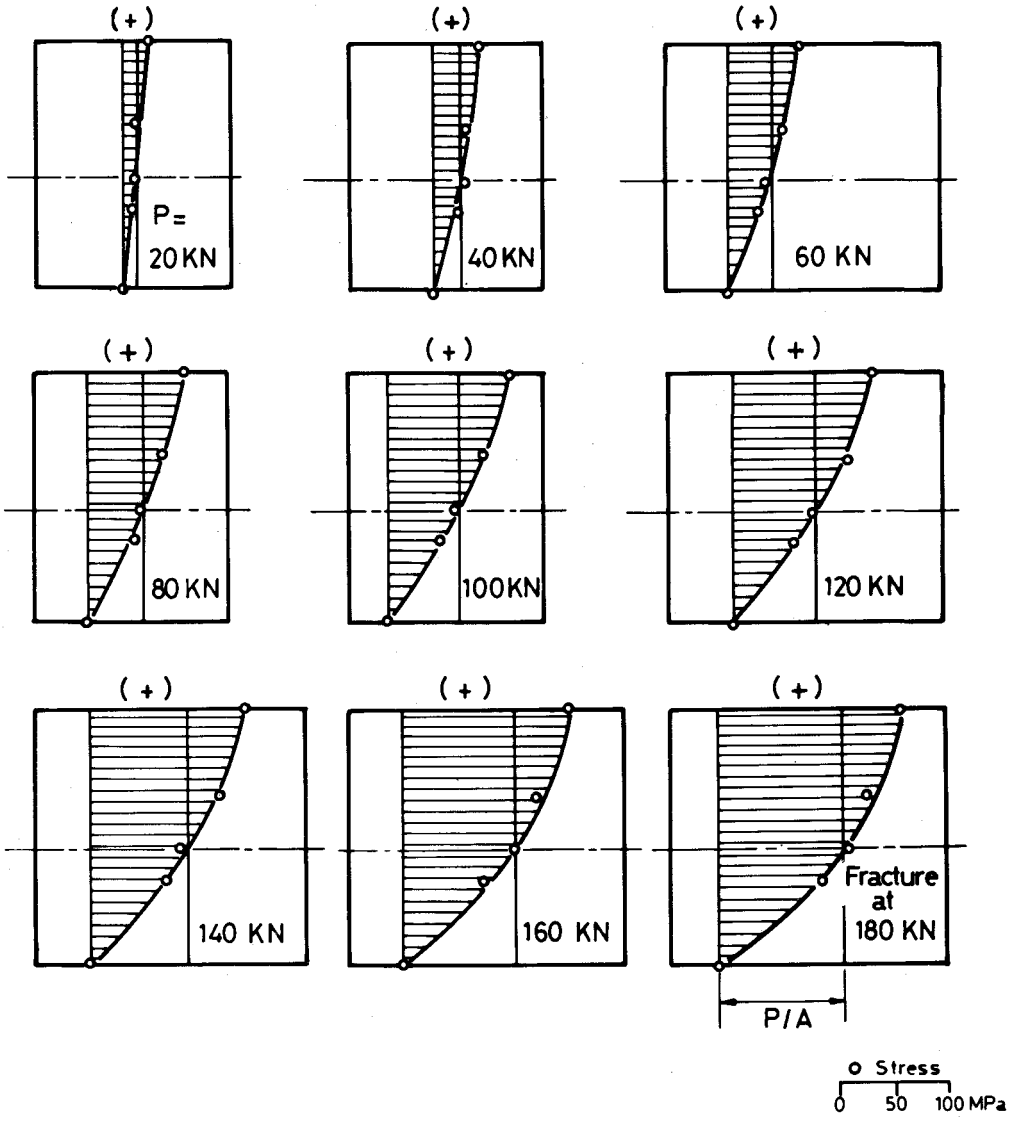

Fig. (7) – Stress distribution for trapezoidal specimens subjected to eccentric **axial loading (e = 8 mm)**
(Case of $| \sigma_2 / \sigma_t | \approx 1$)

Examination of fracture shows that two modes may well be identified, namely:

1) For specimens with relatively high eccentricity values (e.g. e = 45, 88 mm) for which both $|\sigma_1 / \sigma_t|$ and $|\sigma_2 / \sigma_t| > 2$, fracture is mainly characterised by separation on a cleavage plane on the extension side, followed by shearing and slipping along a plane inclined some 65° to the specimen's axis. This is the case of ruling bending stress component.

2) For specimens with relatively low eccentricity values (e.g. e = 6, 8 mm) for which the contribution of the tensile stress component is more dominant than that of the bending stress component i.e. for $|\sigma_2/\sigma_t| \leq 1$, fracture is shown to assume a typical separation with a slightly shearing portion which disappears as the bending to tensile stress ratio becomes equal to or less than 2:

$$\left|\frac{\sigma_b}{\sigma_t}\right| \leq 2,$$

This indicates that the condition: $|\sigma_b / \sigma_t| = 2$ constitutes some demarkation boundary between the two modes of failure encountered in present investigations.

Moreover, the neutral axis would, according to the flexural formula, assume a position midway between the centroidal axis and the extreme compression fibre, Fig. (10). Under these circumstances, while the compressive stress is almost linearly proportional to strain, the tensile stress is no longer proportional to strain, This feature which pertains to grey cast iron can be readily noted in stress profiles displayed in Figs. (4), (5), (8) and (9) for which

$\left|\frac{\sigma_2}{\sigma_t}\right|$ and / or $\left|\frac{\sigma_1}{\sigma_t}\right| > 2.$

This non-linear tensile stress-strain behaviour may be coupled with possible irrecoverable damage in graphite inclusions.

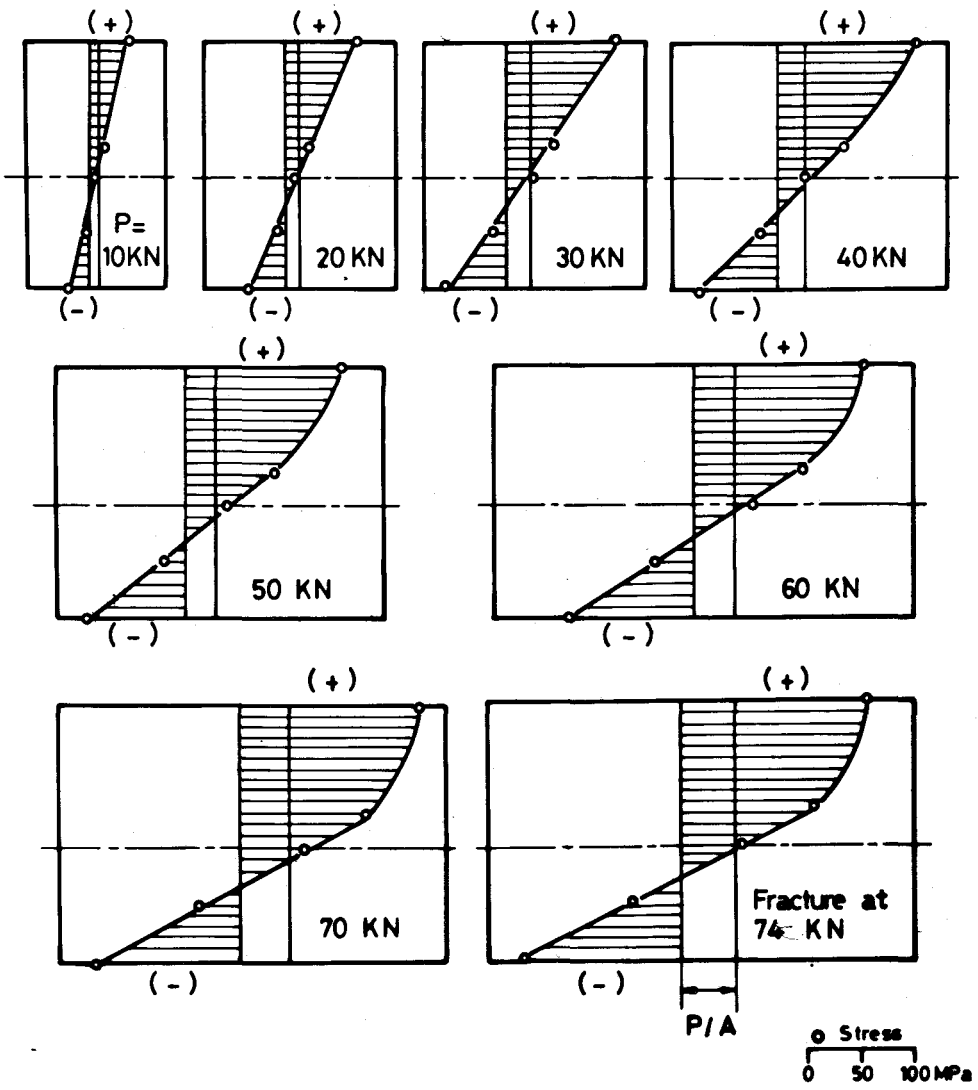

Fig. (8) – Stress distribution for trapezoidal specimens subjected to eccentric axial loading (e = 45 mm)
(Case of both $|\sigma_1 / \sigma_t|$ & $|\sigma_2 / \sigma_t| > 2$)

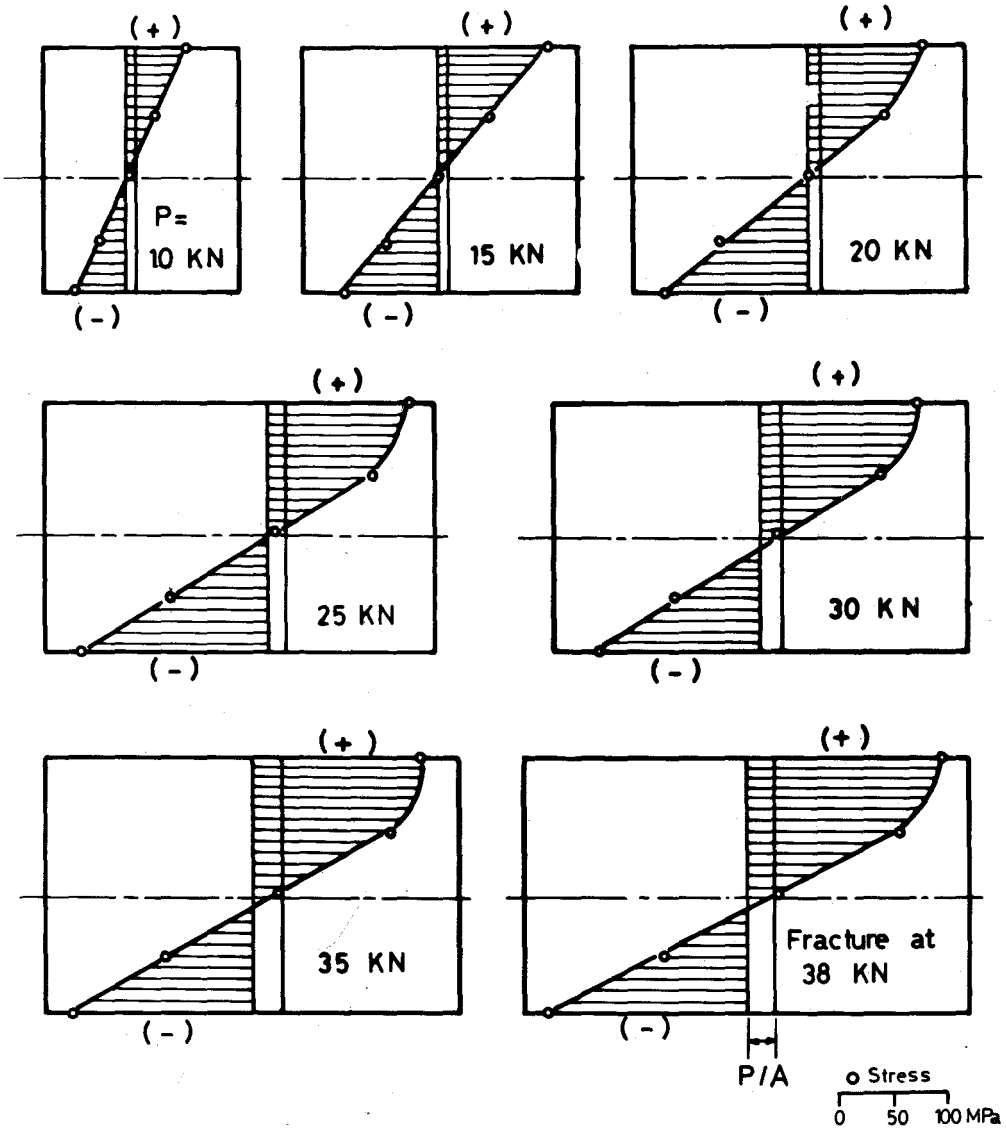

Fig. (9) : Stress distribution for trapezoidal specimens subjected to eccentric axial loading (e = 88 mm)
(Case of both $|\sigma_1 / \sigma_t|$ & $|\sigma_2 / \sigma_t| > 2$)

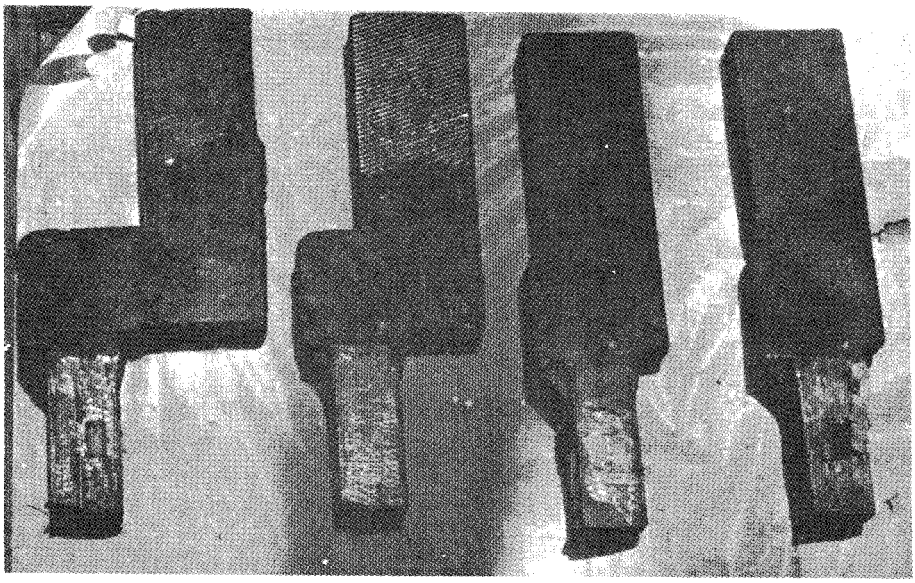

Plate (1) - Typical fractured specimens.

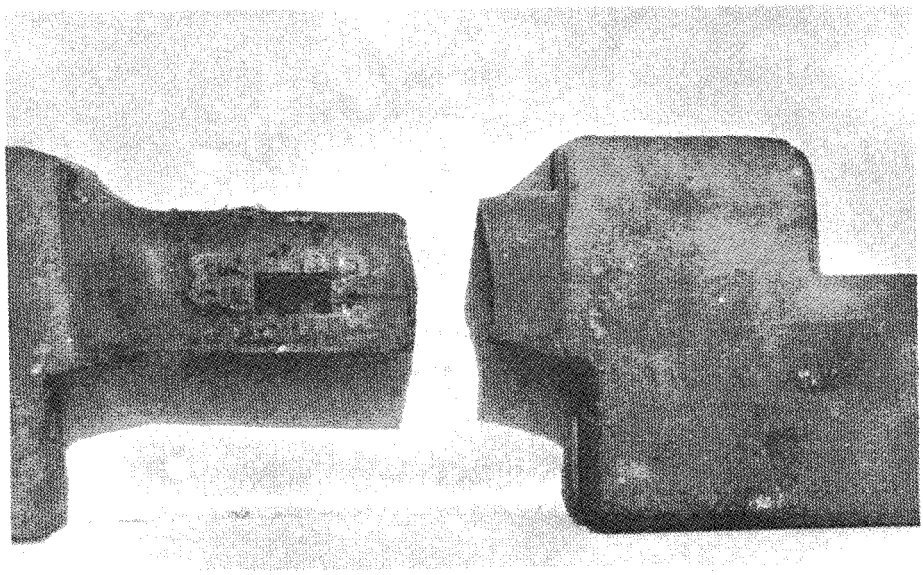

Plate (2) - Enlarged view of fully fractured specimen.

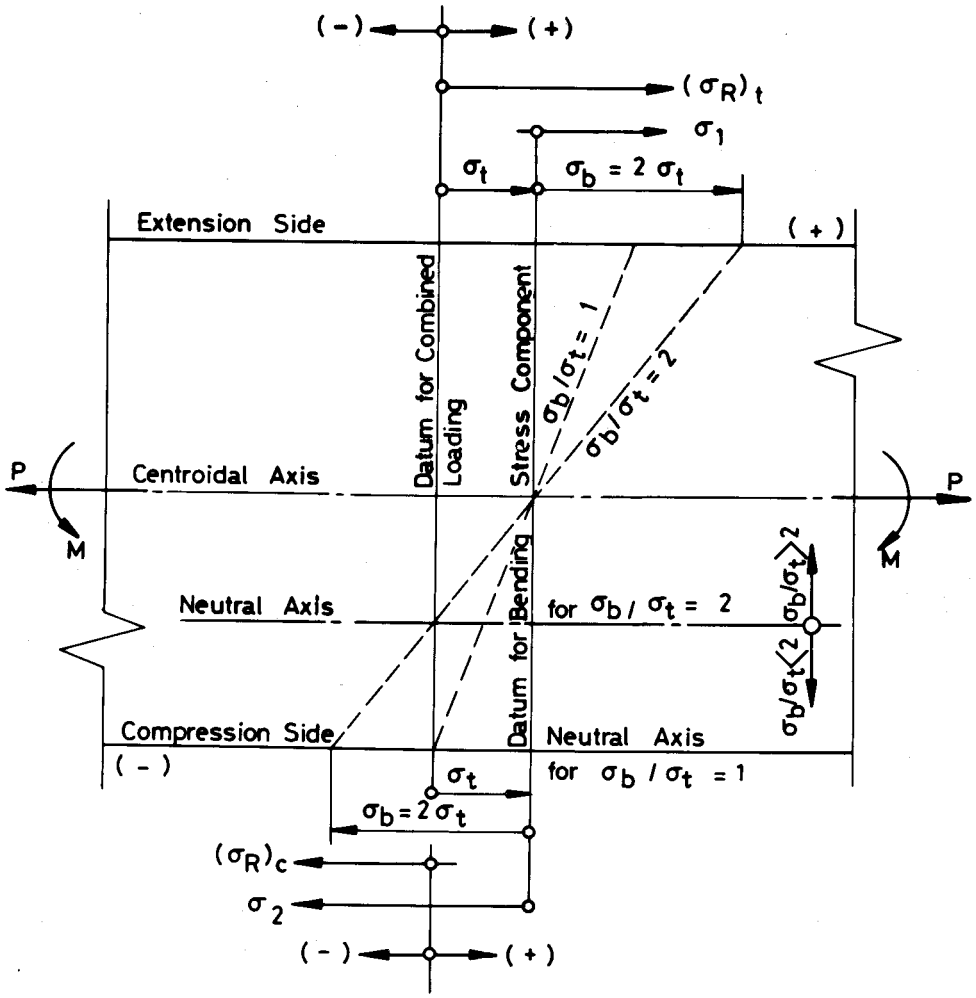

Fig. (10) – Stress patterns based on the flexural formula : $\sigma_b = M.Y/I$.

Table (2) - Stress Values on both Extension and Compression Sides as obtained at the Instant of Fracture.

Specimen's Section (Height = 45 mm)	Load Eccentricity e mm	Stress values on Extension side at Fracture MPa						Experimental Stress values on Compression side measured at Fracture MPa		
		Stress prediction according to linear flexural formula MPa			Experimental stress values MPa					
		σ_t	σ_b	$\sigma_R = (\sigma_t+\sigma_b)$	σ_t	σ_1	$(\sigma_R)_t = (\sigma_t+\sigma_1)$	σ_t	σ_2	$(\sigma_R)_c = (\sigma_2-\sigma_t)$
Rectangular (21x45)	15	87.83	175.66	263.49	80	90	170	80	-190	-110
	40	62.43	332.98	395.41	60	110	170	60	-197.5	-137.5
Trapezoidal (25/45x45)	6	130.16	117.23	247.39	128.5	44	172.5	128.5	- 88.5	+ 40
	8	114.29	137.26	251.55	110	55	165	110	-110	0.0
	45	46.98	317.39	364.37	51	119	170	51	-190	-139
	88	24.13	318.73	342.86	25	150	175	25	-203	-178

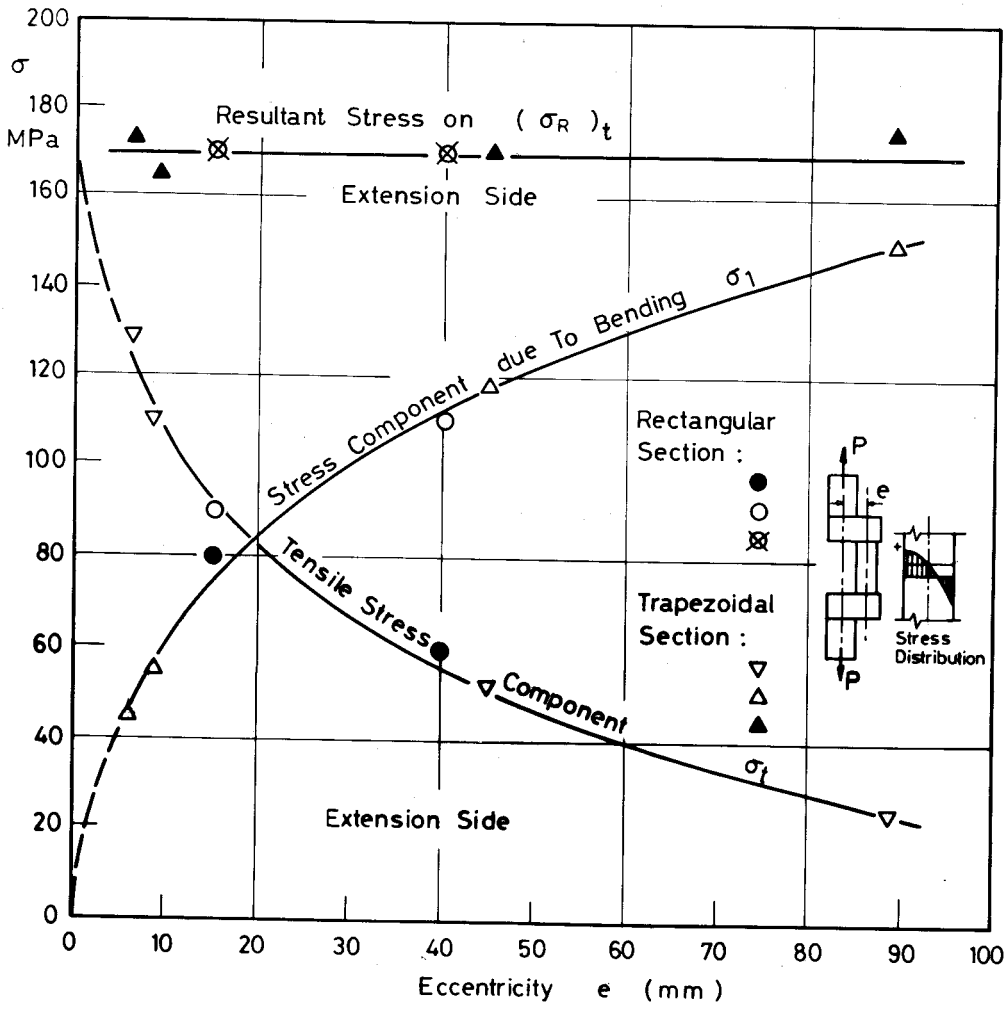

Fig. (11) a

Fig. (11) – Effect of eccentricity [e] on component and resultant stresses at fracture:

(a) On Extension side (b) On Compression side

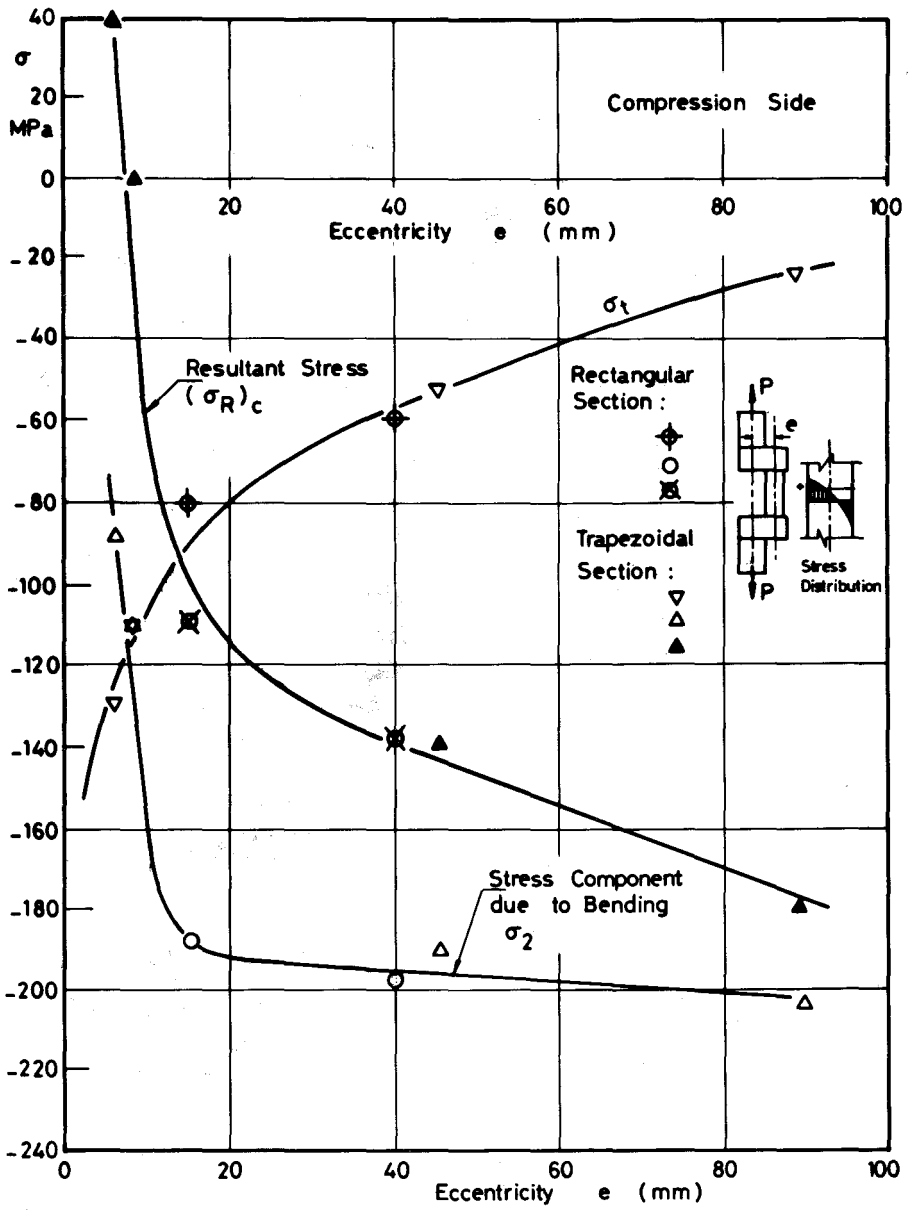
σ
MPa
40
20
0
-20
-40
-60
-80
-100
-120
-140
-160
-180
-200
-220
-240
Compression Side
20
40
60
80
100
Eccentricity e (mm)
σt
Resultant Stress
(σR)c
Rectangular
Section :
Trapezoidal
Section :
P
e
P
Stress
Distribution
Stress Component
due to Bending
σ2
0
20
40
60
80
100
Eccentricity e (mm)

Fig. (11) b

3.3 – Component and Resultant Stresses at Fracture

Stress values at fracture are reproduced in Table (2) for the two types of sections investigated. The effect of eccentricity [e] on component and resultant stresses at fracture are shown in Fig. (11)a for the extension side and in Fig. (11)b for the compression side.

On the extension side, failure seems to take place when the resultant stress $(\sigma_R)_t$ attains the ultimate tensile strength. Owing to the fact that the ultimate compressive strength of grey cast iron is some 2.4 to 4 times its ultimate tensile strength, the resultant stress at the compression side did not herein attain the ultimate compression strength of the material.

The overall stress situation for combined tension and bending at fracture is summed up in Fig. (12) in which stresses and stress ratio zones are indicated, viz. $| \sigma_1 / \sigma_t |$ and $| \sigma_2 / \sigma_t | \lesssim 2$ also ≤ 1.

It is evident that, on the extension side, the bending stress component σ_1 is inversely proportional (in a linear form) to the tensile stress component σ_t = P/A, the sum of the two stress components $(\sigma_R)_t = (\sigma_t + \sigma_1)$ attaining the ultimate tensile strength of the material, under which condition fracture takes place, through initiation and propagation of cracks.

On the compression side, however, the component stress due to bending σ_2 consistently exceeds (numerically) the component stress due to bending on the extension side σ_1, this being associated with the shift of neutral axis away from the centroidal axis in direction of the compression side. The resultant stress $(\sigma_R)_c$ would thus assume positive to zero stress (for e = 6 & 8 mm respectively), the tensile stress component σ_t being the dominating stress. With enhanced load eccentricity [e], the resultant stress $(\sigma_R)_c$ eventually surpasses (numerically) the ultimate tensile strength of the material (about 170 MPa), Fig. (12). Owing to the supremacy of grey cast iron in compressive strength, however, fracture is witnessed by the attainment of ultimate tensile strength on the extension side.

3.4 – Ratio of Bending to Tensile Stress Components

As the ratio of bending to tensile stress components $(\sigma_b / \sigma_t \ , \ \sigma_1 / \sigma_t)$ has been shown to identify the mode of failure, a closer insight into this criterion is herein sought.

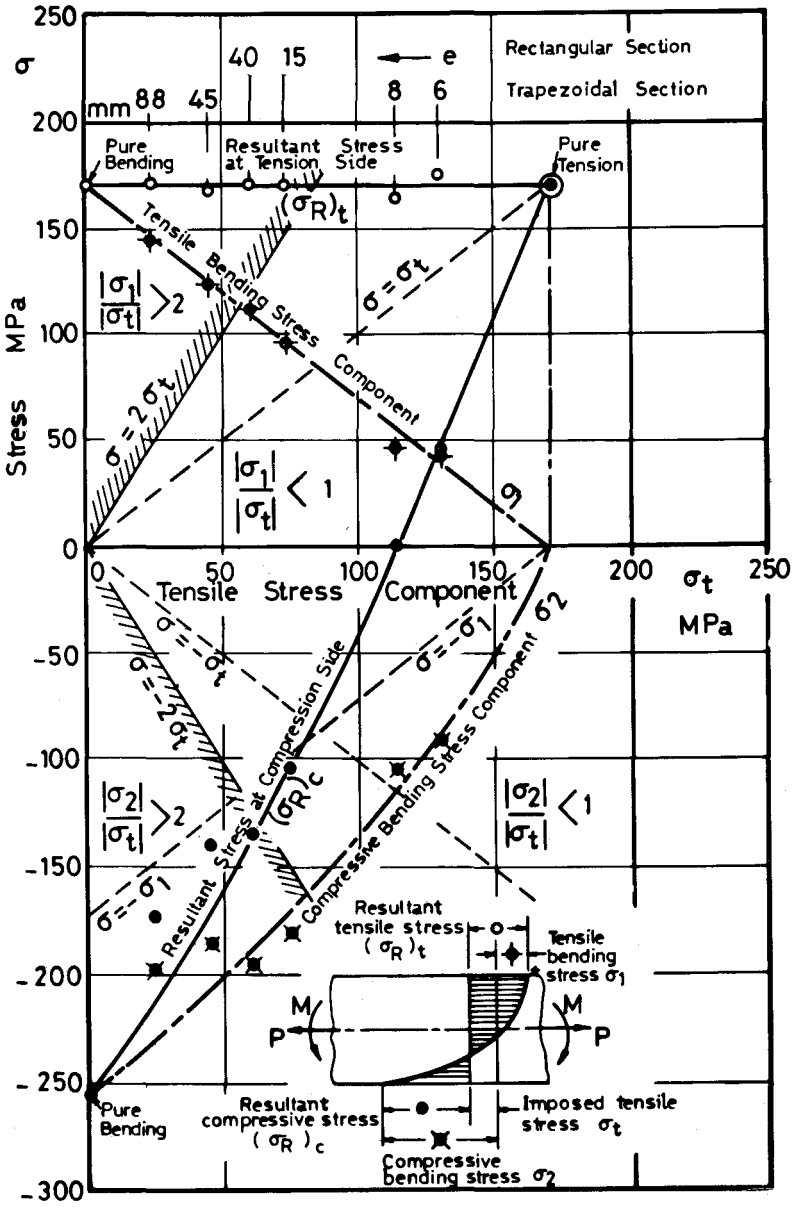

Fig. (12) – Component and resultant stresses on both extension and compression sides at fracture.

Table (3) - Analytical versus Experimental values of the stress ratio $[\sigma_b/\sigma_t]$ and $[\sigma_1/\sigma_t]$ respectively.

Section (Height = 45 mm)		$[\sigma_b/\sigma_t]$ versus $[\sigma_1/\sigma_t]$ for e [mm] =					
		6	8	15	40	45	88
Rectangular (21 x 45)	Analytical* (σ_b/σ_t)	--	--	2	5.333	--	--
	Experimental (σ_1/σ_t)	--	--	1.125	1.667	--	--
Trapezoidal (25/45 x 45)	Analytical* (σ_b/σ_t)	0.9007	1.2010	--	--	6.7554	13.2106
	Experimental (σ_1/σ_t)	0.342	0.5	--	--	2.333	6

* Based on the simple flexural formula : $\sigma_b = M.Y/I.$

For the rectangular section : $\sigma_b/\sigma_t = [6\frac{e}{h}]$.

For the trapezoidal section : $\sigma_b/\sigma_t = 1.1259\ [6\frac{e}{h}]$.

Experimental values of the stress ratio [σ_1 / σ_t] are shown to be, in fact, very much less than the analytical values calculated on basis of the simple linear flexural formula (σ_b = M.Y/I), Table (3). This deviation may be attributed to the shift of the neutral axis towards the compression side and to the non-linearities and the inequalities in stress-strain relations in tension and compression. This behaviour explains the apparent superiority of grey cast iron when subjected to bending.

4 - SUMMARY AND CONCLUSION

Grey cast iron specimens of rectangular and trapezoidal sections were tested under combined bending moment and tensile load. Specimens were made in cranked form with various values of eccentricity of section with respect to load line.

Stress distributions across specimens were obtained, by means of strain gauges, for increasing values of combined loading up to fracture.

For relatively low values of eccentricity, the tensile stress component due to axial load is shown to play the dominating role, with no compression stress acting anywhere in the section. Under such conditions the fracture is entirely tensile with the crack, initiated on the extension side, propagating instantaneously and heading towards rupture as the stress level attains the ultimate tensile strength of the material.

For higher eccentricity values however, the ratio of bending to tensile stress components approaches and surpasses the value 2, with the bending stress component ruling and giving rise to significant compressive stress on the compression side. Nevertheless this latter stress did not, in present investigations, lead to fracture at the compression side as the compressive strength of grey cast iron by far exceeds its strength in tension.

Two modes of fracture are herein identified depending on whether the ratio of bending to tensile stress components is above or below 2, at which value the neutral axis assumes some position midway between the centroidal axis and the extreme compression fibre.

Experimental values of the ratio of bending to tensile stress components are shown, as expected, to be very much lower than the values predicted by the simple linear flexural formula.

This unique behaviour of lamellar graphite cast iron seems to emerge from the non-linearities and the inequalities of stress-strain relations in tension and in compression. For values of the ratio of bending to tensile stress components 2, tensile stress at the extension side ceases to keep its proportionality to strain, while the compression stress, on the other side, maintains its linear proportionality with strain. This may well explain the apparent superiority of grey cast iron in bending with respect to tension.

NOTATION:

A	:	Cross sectional area of specimen
b	:	Width of cross section of specimen
h	:	Height of cross section of specimen
HB	:	Brinell Hardness Number
I	:	Second moment of area of specimen's section about its centroidal axis
M	:	Applied bending moment
P	:	Applied tensile load
x,y,z	:	Cartesian coordinates
Y	:	Coordinate of extreme fibre
Δ	:	Shift of neutral axis away from the centroidal axis, Fig. (1)
ρ	:	Radius of curvature of elastic line, Fig. (1).
σ	:	Normal stress
σ_1 σ_2	:	Actual extreme tensile and compressive stress values resulting from pure bending, Fig. (2)
σ_t	:	Normal stress resulting from the application of tensile load: $\sigma_t = P/A$
σ_b	:	Bending stress component (for the case of simple flexural formula: $\sigma_b = M.Y/I$).

$(\sigma_b)_c$: Bending stress component at compression side

$(\sigma_b)_t$: Bending stress component at extension side

σ_R : Resultant stress

$(\sigma_R)_c$: Numerical value of resultant stress at the compression side: $(\sigma_R)_c = (\sigma_2 - \sigma_t)$, Fig. (2)

$(\sigma_R)_t$: Numerical value of resultant stress at the extension side: $(\sigma_R)_t = (\sigma_t + \sigma_1)$, Fig. (2)

$(\sigma_u)_c$: Ultimate compressive strength of the material

$(\sigma_u)_t$: Ultimate tensile strength of the material

ϕ : Slope of elastic line, Fig. (1)

ACKNOWLEDGMENT

The author wishes to place on record his gratitude to Dr. S.A.R. Naga of Zagazig University, Egypt for supervising the tests.

REFERENCES

1. Shawki, G.S.A. and Naga S.A.R.: "On the Mechanics of Grey Cast Iron Under Pure Bending", Transactions of the American Society of Mechanical Engineers, Journal of Engineering Materials and Technology, New York, Vol. 108, (1986), 2, pp. 141–146.

2. Shawki, G.S.A. and Naga, S.A.R.: "On the Mechanism of Fracture in Grey Cast Iron", Transactions of the American Society of Mechanical Engineers, Journal of Engineering Materials and Technology, New York, Vol. 109, (1987), 4, p. 288–292.